– 3 –

Generation of Ultrashort Laser Pulses

Lasers are divided into *continuous wave lasers* (*cw*) and *pulsed lasers*. In *cw* lasers, the intensity of the emitted light is constant as a function of time. In the *cw* regime, the gain is equal to losses after the round-trip time in the resonator. The value of B in eq. (1.25), for which $G^{(2)} = 1$, is called the *threshold gain*, B_t. When the gain achieved after the round-trip time in the resonator, $G^{(2)} > 1$, every subsequent passage leads to further *amplification* of the light emitted by the laser. This condition is required for pulsed lasers.

The temporal pulse duration in *cw* lasers goes to infinity. In pulsed lasers, the energy is emitted in the form of a short pulse of light. Initially, in 1960, laser pulses were around 10 μs long with a peak power of kilowatts (1 kW = 10^3 W). Shortly after 1960, the *Q-switching technique* reduced the pulse duration by a factor of 10^4 to nanoseconds (1 ns = 10^{-9} s), with peak powers of megawatts (1 MW = 10^6 W). Unfortunately, we cannot produce pulses shorter than 10 ns by this method, because of the required pulse build-up time. The *cavity dumping* technique may reduce the pulse duration to 1–2 ns. These pulses are still too long for monitoring the dynamics in molecular systems because the fundamental chemical processes of life, such as proton transfer, electron transfer, photosynthetic reactions, or the folding of protein molecules, occur on the pico- and femtosecond (1 ps = 10^{-12} s, 1 fs = 10^{-15} s) time-scale.

In 1964, the development of the *modelocking technique* reduced the pulse duration to picoseconds and pushed the peak power up to gigawatts (1 GW = 10^9 W). Shortly thereafter, pulses of just a few femtoseconds were produced using *colliding-pulse modelocking*. Until about a decade ago, dye lasers were used exclusively to generate ultrashort pulses. Now, they have been replaced by the more convenient technology of solid-state lasers and fiber lasers. The lasers working in the modelocking regime represent a special group of continuous wave lasers.

The breakthrough came in 1987 when the current methods of compressing laser pulses were first developed. The idea of *chirped pulse amplification* (CPA), combined with the employment of a solid-state material almost ideal for amplification—Ti:sapphire—led to the production of sub-5-fs pulses at nanojoule energies (1 nJ = 10^{-9} J) that can be amplified to millijoules (1 mJ = 10^{-3} J) with peak powers of terawatts (1 TW = 10^{12} W). The commercial introduction in 1990 of the solid-state Ti:sapphire lasers, which produce femtosecond pulses through *Kerr-lens* *modelocking*, began a revolution in the field of ultrafast research and applications. The past decade has brought further spectacular progress in the development of ultrashort, powerful laser pulses. The femtosecond pulses have been superseded by attosecond pulses (1 as $= 10^{-18}$ s), and peak powers of petawatts (1 PW $= 10^{15}$ W) can be achieved. Femtosecond pulses have durations with the period of molecular oscillations whereas attoseconds are comparable with the periods of electrons revolving in atomic orbitals. A femtosecond pulse's interaction with an electronic wave packet under well-defined conditions gives rise to the generation of higher-harmonics, up to the soft X-ray region, with pulse durations reaching the attosecond region. Clearly, the limits have not been reached yet.

The progress in the development of ultrashort, powerful laser pulses has opened up an exciting area of potential applications such as energy production with laser beams used to ignite a pellet of fusion fuel, or experiments in basic physics to mimic the conditions within the center of stars. It is possible that ultrashort-pulse lasers will help investigations of the processes governing the evolution of stars and their explosion into Supernovae.

As we have learned from this Introduction, modelocking is an extremely important technique for generating ultrashort pulses. In the next section, we will explain what modelocking means, and how ultrafast pulses can be generated.

3.1. MODELOCKING. RELATIONSHIP BETWEEN LINEWIDTH OF STIMULATED EMISSION AND PULSE DURATION

In a free-running regime as discussed so far, lasers produce waves with a mixture of transverse and longitudinal modes, with a random mode-to-mode phase relationship that changes with time. This is not surprising, because coherence is only a single-mode feature. Each mode oscillates independently of the other modes. The intensity of the signal in the free multimode regime that results from the interference of longitudinal modes with random-phase relationships is a chaotic sequence of fluctuations that looks like the characteristics of thermal noises (Fig. 3.1a). The *free-running* laser output is a time-averaged statistical mean value of the intensity.

Suppose that it is possible to achieve a situation where the phases of the longitudinal modes are forced to maintain a fixed phase-relationship to each other. Such a laser is said to be *modelocked* or *phase-locked*. How to achieve this is different matter, which we will discuss later. We will show that, in this case, the laser output shows a periodic repetition of a wave-packet resulting from the constructive interference of longitudinal modes (Fig. 3.1b). The sequence of regular pulses occurs with the period $T = 2L/c$ whereas the single pulse's temporal duration, t_p, is given by

$$t_p = \frac{T}{N} = \frac{2L}{cN}, \tag{3.1}$$

where N is the number of modes generated in an optical resonator (Fig. 3.2), L is the length of the resonator, and c is the speed of the light. Experimental techniques that will be discussed later stimulate the maintenance of a fixed phase-difference between modes, and leads to a laser work-regime called *modelocking*. Therefore, the modelocking results in a train of pulses with the repetition period, T, equal to the

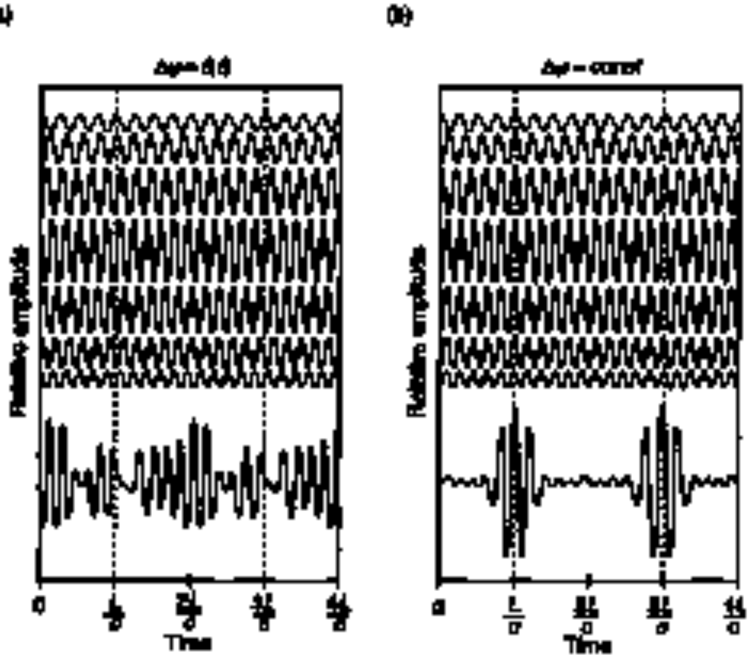

Fig. 3.1 (a) Time-evolution of the electric field in a free-running laser working in a multimode regime; (b) time-evolution of the electric field in a modelocked laser [1].

round-trip time in the optical resonator, and the pulse's temporal duration, t_p, equal to the round-trip time divided by the number of phase-locked modes, N.

As was shown earlier, in eq. (2.6), the number of modes, N, depends on the stimulated emission line width, $\delta\lambda$,

$$N = \frac{4L\delta\lambda}{\lambda_0^2}. \tag{3.2}$$

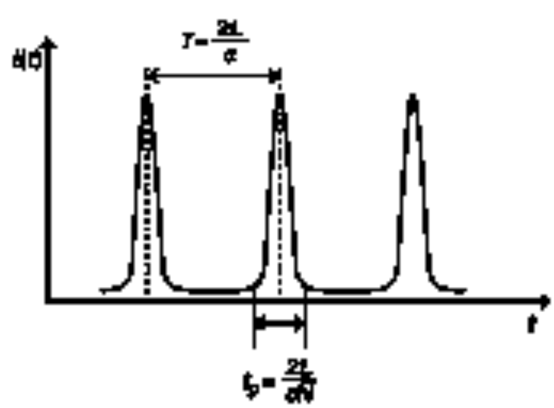

Fig. 3.2 Time-evolution of the intensity in a modelocked laser.

Equations (3.1) and (3.2) indicate that the spectral bandwidth of an active medium, and the laser action threshold, determine the duration of the modelocked pulse. The pulse duration depends on the number of longitudinal modes, N, which in turn depends on the bandwidth of the laser gain, $\delta\Omega$. As a rule, the greater the number of longitudinal modes involved in a broader spectral transition, the shorter is the modelocked pulse. The number of longitudinal modes can vary from a few—in gas lasers (for example in He-Ne lasers)—to around 10^4 or more in dye lasers and in some solid-state lasers, such as the titanium-sapphire laser. In dyes, the fluorescence lines are broad, which generates a large number of longitudinal modes, N, and therefore picosecond and femtosecond pulses can be generated. For gas lasers the emission line is narrow and, as a consequence, pulses shorter than nanoseconds cannot be generated. Fluorescence bands in solid-state lasers are much broader than in gases, owing to inhomogeneous broadening, and picosecond pulses can be generated (e.g., in Nd:YAG). There is a special class of solid-state lasers (vibronic lasers) in which coupling between electrons and vibrational degrees of freedom leads to a considerable band-broadening of spectral lines and, as a consequence, makes it possible to generate femtosecond pulses. The titanium–sapphire laser is the best candidate among the vibronic lasers for producing ultrafast pulses. Detailed discussion of the various types of lasers can be found in the next Chapter.

We will show now that in the modelocking regime one obtains a pulse sequence with the periodicity of $T = 2L/c$, with the duration of an individual pulse being $t_p = 2L/cN$. We shall assume for simplicity that the generated modes are plane waves, $E(t) = E_0 e^{i\omega_0 t}$. This indicates that the spectral distribution of an individual longitudinal mode is described by the Dirac delta function $\delta(\omega - \omega_0)$ with infinitely narrow width. We will apply this approximation, which is not too bad if we recall one of the properties of the Fourier transform. The spectral line of width $\Delta\omega$ (Fig. 3.3a) corresponding to the damped signal in the time domain (Fig. 3.3b) measured in infinite time interval (0, ∞) can be replaced by a non-damped signal in the finite time interval $(-\tau/2, +\tau/2)$ (Fig. 3.3c). Therefore, the plane wave is a reasonable approximation.

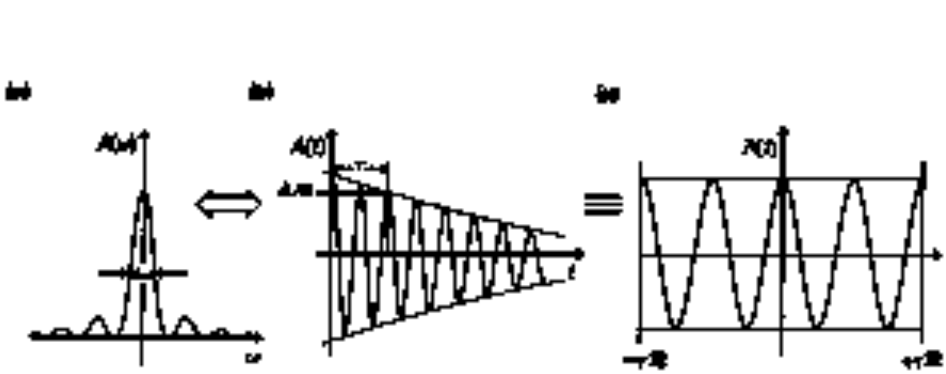

Fig. 3.3 Relationship between the spectral line width $\Delta\omega$ in the frequency domain (a) and the signal in the time domain (b). The signal (b) is equivalent to the signal (c). Explanation in the text.

The total electric field coming from $N = 2n+1$ modes is represented by a sum

$$E(t) = \sum_{k=-n}^{n} E_0 \exp\{i[(\omega_0 + k\Delta\omega_q)t + k\Delta\varphi_q]\}, \tag{3.3}$$

where $\Delta\omega_q$ and $\Delta\varphi_q$ are respectively the frequency and the phase difference between the neighboring longitudinal modes. We now use the following relationships

$$\sum_{k=-n}^{n} e^{ik\alpha} = 2\sum_{k=0}^{n} \cos k\alpha - 1 \tag{3.4}$$

$$\sum_{k=0}^{n} \cos k\alpha = \frac{\cos\frac{n\alpha}{2}\sin\frac{(n+1)\alpha}{2}}{\sin\frac{\alpha}{2}}. \tag{3.5}$$

Substituting (3.4) and (3.5) into (3.3), one obtains

$$\begin{aligned}
E(t) &= E_0 \exp(i\omega_0 t) \sum_{k=-n}^{n} \exp[i(k\Delta\omega_q t + k\Delta\varphi_q)] \\
&= E_0 \exp(i\omega_0 t)\left[2\sum_{k=0}^{n}\cos(k\Delta\omega_q t + k\Delta\varphi_q) - 1\right] \\
&= E_0 \exp(i\omega_0 t)\left[\frac{2\cos\left(n\frac{\Delta\omega_q t+\Delta\varphi_q}{2}\right)\sin\left[(n+1)\frac{\Delta\omega_q t+\Delta\varphi_q}{2}\right]}{\sin\frac{\Delta\omega_q t+\Delta\varphi_q}{2}} - 1\right]
\end{aligned} \tag{3.6}$$

By inserting, $\alpha = (\Delta\omega_q t + \Delta\varphi_q)$ into (3.6) one obtains

$$\begin{aligned}
E &= E_0 \exp(i\omega_0 t)\left[\frac{2\cos\frac{n\alpha}{2}\sin\frac{(n+1)\alpha}{2} - \sin\frac{\alpha}{2}}{\sin\frac{\alpha}{2}}\right] \\
&= E_0 \exp(i\omega_0 t)\frac{2\cos\frac{n\alpha}{2}\left(\sin\frac{n\alpha}{2}\cdot\cos\frac{\alpha}{2} + \cos\frac{n\alpha}{2}\cdot\sin\frac{\alpha}{2}\right) - \sin\frac{\alpha}{2}}{\sin\frac{\alpha}{2}} \\
&= E_0 \exp(i\omega_0 t)\frac{\cos\frac{2n\alpha}{2}\sin\frac{\alpha}{2} + \sin\frac{2n\alpha}{2}\cos\frac{\alpha}{2}}{\sin\frac{\alpha}{2}} \\
&= E_0 \exp(i\omega_0 t)\frac{\sin\frac{(2n+1)\alpha}{2}}{\sin\frac{\alpha}{2}}
\end{aligned} \tag{3.7}$$

Since $2n+1 = N$ is equal to the number of longitudinal modes, one can write

$$E = E_0 \exp(i\omega_0 t)\frac{\sin\frac{N(\Delta\omega_q t+\Delta\varphi_q)}{2}}{\sin\frac{(\Delta\omega_q t+\Delta\varphi_q)}{2}}. \tag{3.8}$$

If the phase-difference between the neighboring longitudinal modes, $\Delta\varphi_q$, changes with time in a random way, the resultant electric field, E, in eq. (3.8) changes chaotically with time as in Fig. 3.1a. However, if the phase difference, $\Delta\varphi_q$, between modes is

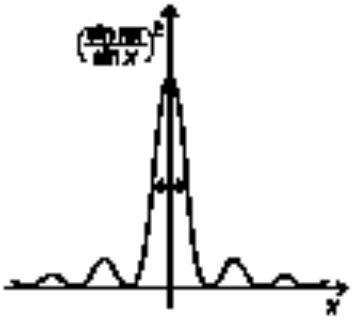

Fig. 3.4 Profile of a function $\left(\frac{\sin Nx}{\sin x}\right)^2$.

constant, the total intensity of the electric field, E, arising as a result of the interference from N synchronized longitudinal modes, is an amplitude-modulated wave at a carrier frequency ω_0, equal to the central mode with the envelope expressed in the form

$$A(t) = E_0 \frac{\sin N(\Delta\omega_q t + \Delta\varphi_q)/2}{\sin(\Delta\omega_q t + \Delta\varphi_q)/2}. \tag{3.9}$$

The intensity, $I(t) = A^2(t)$, generated as a result of the interference between the N modes is a function of type $\left(\frac{\sin Nx}{\sin x}\right)^2$, well known from diffraction theory, with the maximum at $x = 0$ illustrated in Fig. 3.4.

Since the function (3.9) is periodic, the radiation intensity generated as a result of the interference of N synchronized longitudinal modes is a repetition of pulses, periodic in time, as represented in Fig. 3.5.

The result derived in eqn. (3.9) shows that the laser radiation is a sequence of regular pulses with temporal intervals of T, if the phase difference $\Delta\varphi_q$ between the neighboring modes is constant. The temporal intervals, T, between the pulses can be

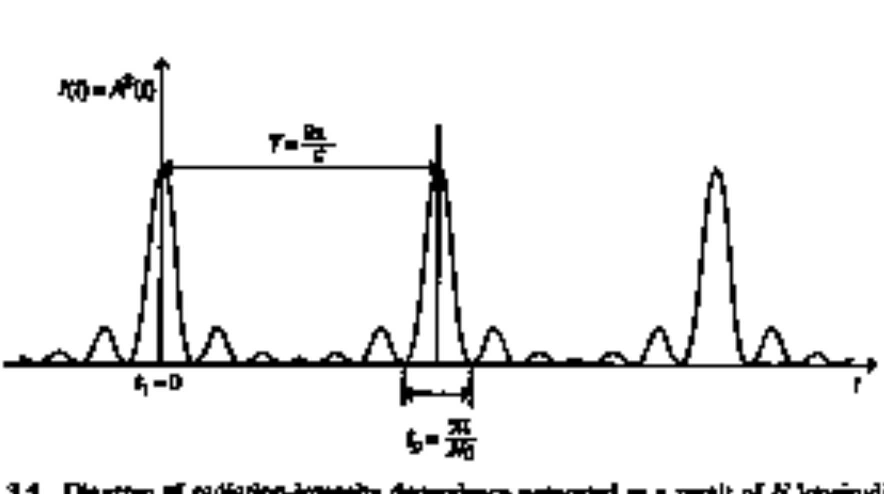

Fig. 3.5 Diagram of radiation-intensity dependence generated as a result of N longitudinal modes' interference, as a function of time.

calculated easily from eq. (3.9). We simply have to find the distance between the two subsequent largest maxima in Fig. 3.5.

From eq. (3.9), the first maximum, at time t_1, occurs when

$$\Delta\omega_q t_1 + \Delta\varphi_q = 0. \tag{3.10}$$

The next maximum, at time t_2, has to fulfil the condition

$$\Delta\omega_q t_2 + \Delta\varphi_q = 2\pi. \tag{3.11}$$

Subtracting the equations (3.11) and (3.10), we obtain $\Delta\omega_q T = \Delta\omega_q(t_2 - t_1) = 2\pi$. Therefore, the interval T between the modelocked pulses is

$$T = \frac{2\pi}{\Delta\omega_q} = \frac{2\pi}{2\pi\Delta\nu_q} = \frac{2L}{c}. \tag{3.12}$$

The equation (3.12) employs the relationship (2.3) derived in Chapter 2 for the frequency difference between the neighboring modes $\Delta\nu_q$, which is $\frac{c}{2L}$. In a similar way, we can estimate a single-pulse duration, t_p. One can see from Figure 3.5 that it corresponds approximately to the distance between the first two minima around the "large" maximum. The minimum occurs when the numerator of eq. (3.9) is equal to zero

$$\sin N(\Delta\omega_q t + \Delta\varphi_q)/2 = 0, \tag{3.13}$$

corresponding to

$$N(\Delta\omega_q t_1 + \Delta\varphi_q)/2 = 0, \tag{3.14}$$

and

$$N(\Delta\omega_q t_2 + \Delta\varphi_q)/2 = \pi. \tag{3.15}$$

Thus, the single-pulse duration, t_p, is

$$t_p = t_2 - t_1 = \frac{2\pi}{N\Delta\omega_q} = \frac{2L}{Nc}. \tag{3.16}$$

Therefore, we have proved that the relationship (3.1) is valid.

By inserting eqn. (3.2) into (3.16), one obtains the pulse duration, t_p, in another form

$$t_p = t_2 - t_1 = \frac{\lambda_0^2}{2cd\lambda}. \tag{3.17}$$

Equation (3.17) is a very important relationship between the pulse duration, t_p, and the gain bandwidth, $d\lambda$ for the stimulated emission. According to this relationship, the broader the spectral width $d\lambda$, the shorter is the pulse that can be generated. We will refer to this relationship many times.

The relationship (3.17) is a consequence of the relationship between the time domain and the frequency domain described by the Fourier transform in eq. (2.14), as is discussed in Chapter 2. It simply illustrates the Heisenberg uncertainty principle

$$\Delta t \Delta E \geq h/2\pi. \tag{3.18}$$

where Δt denotes the uncertainty of the time, which may be interpreted as a pulse duration, t_p, and $\Delta E = \hbar\Delta\omega$ defines the uncertainty of the energy corresponding to the width of the spectral band.

The magnitude of the product $\Delta t \cdot \Delta E$ depends on a temporal pulse shape. We assume that the pulse shape is described by a Gaussian function

$$E(t) = \frac{E_0}{\tau}\exp\left(-\frac{t^2}{2\tau^2}\right). \tag{3.19}$$

The frequency spectrum, $E(\omega)$, can be obtained from the Fourier transform

$$E(\omega) = \frac{1}{2\pi}\int_{-\infty}^{\infty} E(t)e^{-i\omega t}dt = \frac{E_0}{2\pi}\exp\left[-\frac{\tau^2}{2}(\omega-\omega_0)^2\right]. \tag{3.20}$$

This indicates that the shape of the spectral band in the frequency domain is also described by a Gaussian distribution. The full width at half height (FWHH) of the temporal pulse profile $E(t)$ given by (3.19) is

$$\Delta t_{FWHH} = 2\tau(\ln 2)^{1/2}, \tag{3.21}$$

and the FWHH of the spectral profile, $E(\omega)$, in the frequency domain given by eq. (3.20) is

$$\Delta\omega_{FWHH}/2\pi = \Delta\nu_{FWHH} = (\ln 2)^{1/2}/\pi\tau. \tag{3.22}$$

Thus, for the Gaussian profile the product $\Delta t \cdot \Delta E$ is equal to

$$\Delta t_{FWHH} \cdot \Delta\nu_{FWHH} = 0.441. \tag{3.23}$$

For other shapes of temporal profiles, this product is different from 0.441. Table 3.1 shows the values of the product for the most common pulse shapes.

Table 3.1

The product of time and spectral widths, $\Delta t_{FWHH}\Delta\nu_{FWHH}$, for different shapes of temporal pulses, $I(t)$

Function	$I(t)$	$\Delta t_{FWHH}\Delta\nu_{FWHH}$
Square	$I(t) = 1;\ \lvert t\rvert \le t_p/2$ $I(t) = 0;\ \lvert t\rvert > t_p/2$	1.000
Diffraction	$I(t) = \frac{\sin^2\left(\frac{t}{\Delta t_{FWHH}}\right)}{\left(\frac{t}{\Delta t_{FWHH}}\right)^2}$	0.886
Gaussian	$I(t) = \exp\left(-(4\ln 2)t^2/2\Delta t^2_{FWHH}\right)$	0.441
Hyperbolic Secant	$I(t) = \mathrm{sech}^2\left(\frac{1.76t}{\Delta t_{FWHH}}\right)$	0.315
Lorentzian	$I(t) = \frac{1}{1+\left(\frac{4t^2}{\Delta t^2_{FWHH}}\right)}$	0.221
Exponential	$I(t) = \exp\left(\frac{-(\ln 2)t}{\Delta t_{FWHH}}\right)$	0.142

The relationship derived in eq. (3.23) corresponds to an ideal situation of a perfectly modelocked laser with a pulse called the *Fourier-transform limited pulse*. Such a pulse is the shortest pulse, of Δt_{FWHM}, that can be generated for a given gain-spectrum, $\Delta\nu_{FWHM}$. In practice, such pulses are seldom produced. The uncertainty relationship (3.23) holds only when the individual longitudinal modes are perfectly synchronized with each other, or in other words, when the *spectral phase* is a linear function of frequency, as we assumed in eq. (3.3)

$$
\begin{aligned}
E(\omega) &= A(\omega)e^{i\Phi(\omega)} \\
\Phi(\omega) &= \Phi_0 + \Phi_1(\omega - \omega_0).
\end{aligned}
\tag{3.24}
$$

It is crucial for perfect modelocking that all frequency components experience the same round-trip cavity-time, which is ensured by the phase linearity in eq. (3.24). Owing to material dispersion, each frequency component travels with a different velocity (the so-called *group velocity*, which will be discussed in Chapter 5), and the spectral phase is usually more complicated than linear

$$
\Phi(\omega) = \sum_{0}^{\infty} \frac{1}{n!} \frac{d^n\phi}{d\omega^n}\bigg|_{\omega_0} (\omega - \omega_0)^n. \tag{3.25}
$$

Owing to the quadratic term in the phase, each frequency component that comprises the spectrum of the pulse experiences a delay which is linearly proportional to the offset from the central frequency, ω_0. The pulse is said to be "*linearly chirped*". In this case, a Gaussian pulse for an ideal modelocking presented in Fig. 3.6 is replaced by a Gaussian pulse linearly chirped (Fig. 3.7). The linear chirp can be negative or positive (what this means exactly, we will discuss in Chapter 7). One can see from Fig. 3.7 that for the positive chirp, red components travel faster than blue ones, in contrast to the negative chirp.

To produce pulses as short as possible, dispersion in the cavity must be compensated for by adding optical elements—typically pairs of prisms or gratings and, especially, coated mirrors or a length of optical fiber. We will discuss these methods in Chapter 5.

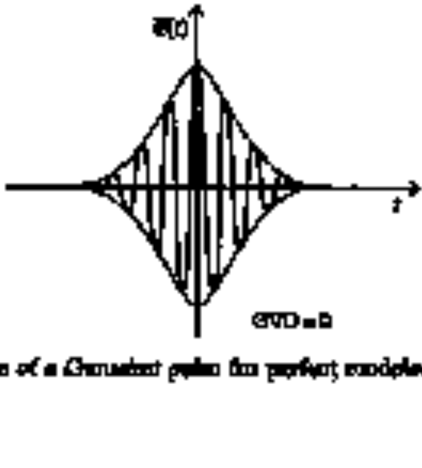

Fig. 3.6 Illustration of a Gaussian pulse for perfect modelocking (zero chirped).

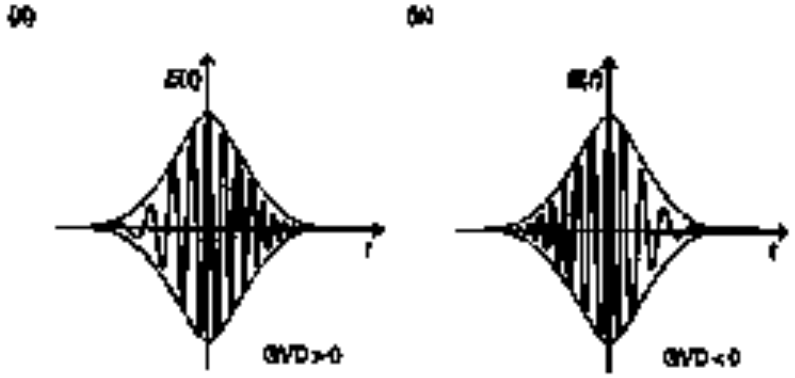

Fig. 3.7 Illustration of a Gaussian pulse with positive (a), and negative (b), chirp.

3.2. METHODS OF MODELOCKING. ACTIVE AND PASSIVE MODELOCKING

The question arises of how to achieve the modelocking, or in other words, how to create a situation with a fixed mode-to-mode phase-relationship between the neighboring modes. There are many different ways of modelocking but the principle is always the same—the periodic modulation of the optical resonator parameters (amplitude or frequency) with a frequency equal to the difference of frequencies between the neighboring longitudinal modes, $\Delta\omega_q$.

Generally, the methods of modelocking can be classified into *active modelocking* and *passive modelocking*. A special case of passive modelocking is the *self-modelocking* which occurs spontaneously in an active medium as a result of self-focusing.

The modulation of the optical resonator parameters with the frequency $\Delta\omega_q$ can be obtained in a variety of methods including:

a) acousto-optic devices which produce a sound wave, modulating the laser beam's intensity propagating through a resonator,
b) electro-optical modulators driven at exactly the frequency separation of the longitudinal modes, $\Delta\omega_q$;
c) the *saturable absorbers* modulating the amplification factor of an active medium.
The first two methods belong to the active modelocking methods, whereas the last represents the passive modelocking.

We now ask, "What is the mechanism which causes the randomly oscillating longitudinal modes to begin oscillating in synchronized phases, under the influence of the modulating factor, at the frequency $\Delta\omega_q$?" This can be achieved only when the longitudinal modes are coupled together. When we modulate the amplitude or frequency of a given longitudinal mode of frequency ω_k, with the modulation frequency Ω, an additional radiation component appears at $\omega_k \pm m\Omega$. If the modulation frequency Ω is equal to the frequency-separation, $\Delta\omega_q$, of the longitudinal modes, these additional components overlap with the neighboring modes, causing coupling of the modes and stimulating oscillations in the same phase.

Here, we will describe the basic aspects of frequency- or amplitude modulation. In the first method, (a), an *acousto-optic* transducer generates a sound wave that modulates the amplitude of the laser beam in the optical resonator. Understanding of the mechanisms governing the interactions between light and sound waves is very important, since the acousto-optic devices are often used in laser technologies—not only for modelocking, but also in pulse-selection (cavity dumping) and in the *Q*-switching amplification.

A brief description of the interactions between light and sound waves is given below. We follow an excellent tutorial discussion in ref. [1]. A more rigorous discussion of these phenomena can be found in ref. [2].

If a transducer emitting ultrasonic waves at frequency Ω in the range of megahertz is placed in a glass of water (Fig. 3.8) illuminated with a laser beam of frequency ω, one notices that the light passing through the glass splits into several beams. At each side of the fundamental beam, which is unaffected in frequency ω and direction, one observes side beams having frequencies $\omega \pm n\Omega$. This phenomenon is named the *Debye and Sears effect*, after the authors who first described it in 1932 [3]. The Debye and Sears effect is similar to light diffraction by a slit. The difference is that in diffraction by a slit all the side beams have the same frequency, ω as the incident beam. Because the sound wave is a longitudinal wave, and its propagation occurs by creating regions of different density (Fig. 3.8), the analogy to diffraction is not surprising, because the regions of compression and dilution generated by the sound wave may remind us of a diffraction grating. Indeed, the regions of dilution can be treated as the slits through which more light passes than through the regions of greater density. However, why do the frequencies $\omega \pm \Omega$, $\omega \pm 2\Omega$, $\omega \pm 3\Omega$ appear? We may imagine that light of frequency ω arrives at a medium characterized by a refractive index n_1 (Fig. 3.9). If the refractive index n_1 is larger than that of the

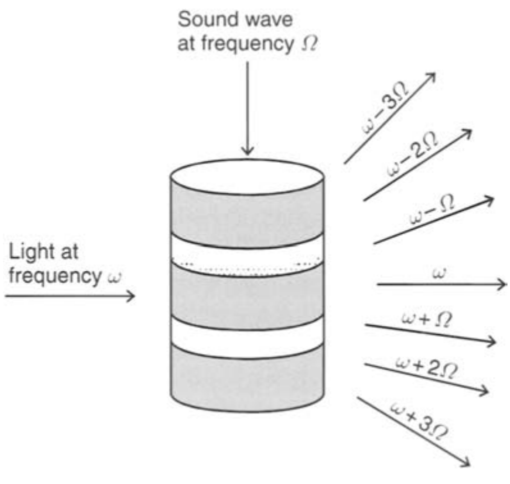

Fig. 3.8 Illustration of light and sound waves interaction.

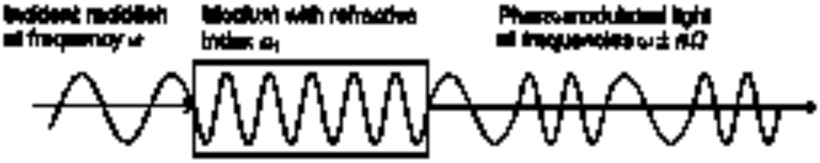

Fig. 3.9 Light modulation by periodic changes of the refractive index, n_1.

environment, n_0, the light in the medium travels n_1/n_0 times slower (since $\lambda\nu = c/n$). Let us assume that we have found a way of modulating the refractive index, n_1, with frequency Ω. This modulation causes the light in the medium to propagate faster or slower, and the output light from the medium is also modulated. The output light is characterized by the carrier frequency, ω, of the incident light and a side frequency of Ω leading to the appearance of additional components at frequencies of $\omega \pm n\Omega$ (Fig. 3.10).

The longer the optical path, l, in the material, the greater are the amplitudes of the sidebands at the frequencies $\omega \pm n\Omega$. The sidebands' amplification is reached at the expense of the amplitude of the fundamental beam at the carrier frequency, ω. The optical pathlength, l, is the parameter defining when the Debye–Sears effect can occur. We can distinguish two limiting cases

$$l \ll \frac{\Lambda^2}{2\pi\lambda} \tag{3.26}$$

and

$$l \gg \frac{\Lambda^2}{2\pi\lambda}, \tag{3.27}$$

where λ is the optical wavelength, and Λ is the length of an acoustic wave. The relationship (3.26) defines the critical length of the optical path for which the Debye–Sears effect can be observed. The relationship (3.26) characterizes the conditions required for modelocking with *acousto-optic devices*, and is called the

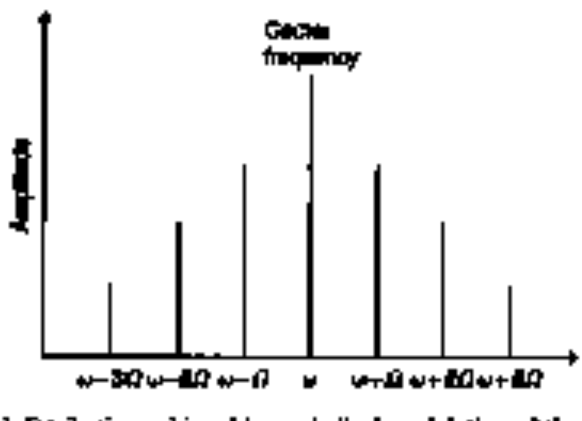

Fig. 3.10 Spectral distribution achieved by periodical modulation of the refractive index at frequency Ω.

Raman–Nath regime after the authors who derived it. The relationship (3.27) is employed in another acousto-optic configuration—a device for pulse selection called *the cavity dumper*, where it defines the conditions for the *Bragg reflection*.

The simplest way to modulate the refractive index n_1 is to make a periodic change of a medium's density, which can be achieved by passing the acoustic wave through the medium. The acoustic wave then creates regions of compression and dilution at the frequency Ω. In real acousto-optic devices, a standing acoustic wave is generated instead of a travelling wave whose forefront moves downward as in Fig 3.8. The standing wave shown in Fig 3.11 remains in place instead of moving down the column, and the refractive index, n_1, at each place in the column (e.g., the dashed line in Fig. 3.11) changes sinusoidally with the frequency Ω. Twice during the cycle the density is distributed uniformly along the whole column (3.11b and 3.11d), and twice it achieves a maximum at which the refractive index, n_1, is largest (3.11a and 3.11e), as well as once when it achieves the minimum density at which the refractive index, n_1, is the smallest (3.11c). Thus, twice during the cycle $T = \frac{1}{\Omega}$ when the density is distributed uniformly, the incident beam passes unaffected and the frequency of the transmitted beam is equal to ω, and the radiation amplitude is equal to the amplitude of the incident light. At other times diffraction occurs, leading to the appearance of additional bands at $\omega \pm n\Omega$, at the expense of weakening the amplitude of the carrier wave at frequency ω. Now we understand why an acousto-optical transducer modulates the amplitude of the light in an optical resonator. If this modulation is held at the frequency equal to the difference between the longitudinal modes, $\Delta\omega_0 = c/2L$, the Debye–Sears effect leads to modelocking.

In practical applications an acousto-optic modulator consists of a small fused-silica (SiO_2) element (prism or plate) placed close to the optical resonator mirror (Fig. 3.12). The prism is used in multimode lasers, e.g., in argon lasers for wavelength selection.

The piezoelectric transducer at one end of a prism or a plate generates an acoustic wave of frequency $\frac{c}{2L}$. The end walls of the prism are polished to provide acoustic

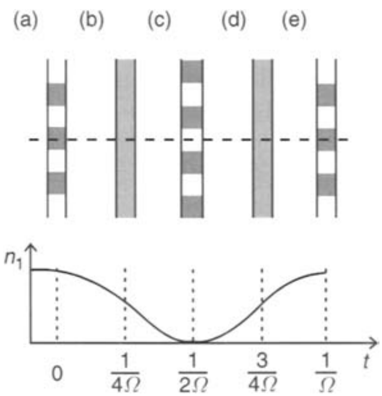

Fig. 3.11 Illustration of periodic changes of the refractive index by changes in the density of the medium caused by a acoustic wave [1]

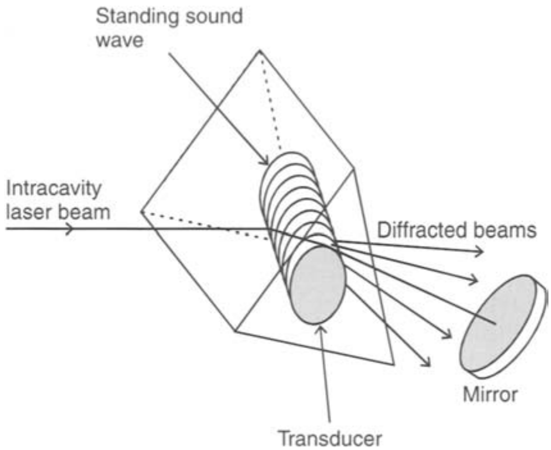

Fig. 3.12 Model of piezoelectric transducer.

resonance to produce the standing acoustic wave inside. A laser beam inside the optical resonator passes through the region of formation of the standing acoustic wave, interacting with it in the manner described above. As a consequence of this interaction, the laser beam with frequency ω is periodically modulated at the frequency $\Omega = \frac{c}{2L}$ by beam tossing from the sidebands at frequency $\omega \pm n\Omega$. Only the axial beam participates in the laser action: the sidebands which are deflected from the main axis will be suppressed, since the length of the optical path for the sidebands is different from L at which the condition $\frac{q\lambda}{2} = L$ is fulfilled.

Traditionally, the acousto-optic modulation is used in flash-lamp pumped solid-state lasers such as Nd:YAG lasers. Recently, acousto-optic modulation has been utilized for Q-switching and modelocking in *diode-pumped solid-state* (*DPSS*) *lasers*.

A continuous-wave actively modelocked laser produces a train of pulses at a repetition rate in the range of 80–250 MHz and energy of a few nJ. If more energy is required, a pulse selected from the train can be amplified in a regenerative amplifier to reach a few mJ, as described in Chapter 4. If a more powerful pulse is needed, techniques that combine simultaneous modelocking and Q-switching or cavity dumping are used. Such a Q-switched and modelocked laser emits a train of modelocked pulses within the envelope of a 100–250 ns Q-switch pulse.

We have just presented the idea of acousto-optic modulation. However, electro-optic devices can serve the same function as acousto-optic modulators both for active modelocking and Q-switching. A *Pockels cell* is a particular example of an electro-optic device. For example, Pockels cells are used to select and route high-peak-power pulses from a modelocked Ti:sapphire laser for *chirped pulse amplification* (*CPA*). We will discuss electro-optic devices in Chapter 6, where we will explain the idea of a *regenerative amplifier* and CPA.

Another way of modelocking is to use passive modelocking and *saturable dye absorbers*. There are various designs of passive modelocking, but a dye inside the resonator is a major requirement. One of many possible configurations is presented

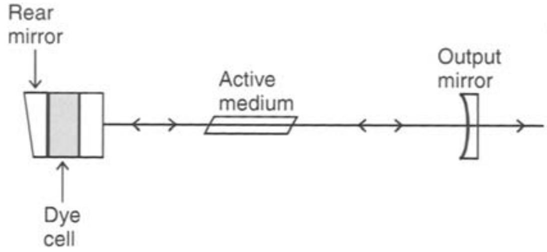

Fig. 3.13 The passive modelocking achieved by the saturable absorbers method.

in Fig. 3.13. In this configuration a dye cell and the rear mirror are combined to reduce the number of reflecting surfaces in the laser cavity, and to minimize unwanted losses.

Let us assume that the absorbing dye in a cell is characterised by the energy levels E_1 and E_2 with $E_2 - E_1 = \hbar\omega$, where ω is the frequency of one of many longitudinal modes in the optical cavity. The lifetime of the absorbing dye molecules in the excited state is taken to be τ. If the lifetime is of the order of magnitude of the cavity round-trip time $T = \frac{1}{\Delta\nu} = \frac{2L}{c}$, i.e., a few nanoseconds in typical resonators, the dye molecules act like a passive Q-switching (see Section 3.3). If the lifetime is comparable to the pulse duration of a modelocked pulse, i.e., a few picoseconds, simultaneous modelocking and Q-switching can occur.

We will show that the dye in a cell plays the role of a filter (or a natural Q-switch shutter). Indeed, light in the optical resonator arriving at the cell-mirror promotes some molecules from the lower level, E_1, to the upper level, E_2, causing losses in the light intensity as a result of absorption by the dye. Initially, just at the beginning of pumping, the laser gain barely overcomes the losses of the saturable dye. In the early stage of pulse generation, the longitudinal modes are not synchronised in phase, and the laser output represents a chaotic sequence of fluctuations. As a result, both the amplification and dye absorption are not very efficient. As the pump process continues to increase the intensity above a threshold, light-amplification in the resonator approaches values of the saturation intensity in the dye. The gain in the laser medium is still linear, but the absorption of the dye becomes non-linear. With absorption of light at the high intensity the substance undergoes saturation (bleaching), so the condition $N_1 = N_2$ is fulfilled (where N_1 and N_2 indicate the number of molecules at the levels E_1 and E_2). The dye in the cell becomes transparent to the laser beam, which can arrive at the reflective rear mirror and back to the active medium, which in turn causes quick gain amplification. Now the intensity is sufficiently high, and the amplification in the medium becomes non-linear. The dye molecules return to the ground state, E_1, after time τ, and the process of light absorption is repeated. Therefore, the transmission in the cavity is modulated by successive passages of the high-intensity pulses resulting in a modelocked pulse train appearing in the laser output. Finally, the population inversion is depleted, and the pulse decays.

To summarise we may say that the mechanism of the passive modelocking with the saturable dyes consists of three main steps: 1) linear amplification and linear dye absorption; 2) non-linear absorption in the dye; 3) non-linear amplification when the dye is entirely bleached.

We have described only the most basic aspects of passive modelocking with saturable absorbers. Deeper treatments of this subject can be found in refs. [4–8]

The passive modelocking with saturable dye absorbers suffers from many inherent shortcomings. The laser outputs obtained with this method can be unpredictable unless the resonator alignment, pumping intensity, and dye concentrations are carefully adjusted. Also, the mixing, handling, and maintaining the proper dye concentration can be cumbersome.

We have shown that saturable dyes can be applied for passive modelocking only when a dye has a lifetime comparable to the duration of modelocked pulses. In practice, this means that the method can be employed only for modelocking of picosecond pulses. If we wish to use this method for shorter, femtosecond pulses, we need a faster "shutter" than a saturable dye. In recent years, the method has been replaced by continuous-wave passive modelocking in solid-state lasers by using *nonresonant Kerr effect—Kerr-lens modelocking* (KLM), or other passive techniques such as *saturable Bragg reflectors* (*SBR*) [9–11].

As long ago as the 1980s, engineers realized that a semiconductor quantum well, which will be described in Chapter 4, could play the role of a saturable absorber. A typical saturable Bragg reflector consists of alternate layers of high and low-index semiconductor materials, which also act as saturable absorber layers (Fig. 3.14).

In one particular configuration, the substrate material is GaAs, with alternate layers of AlAs and AlGaAs forming a multilayer Bragg mirror (Fig 3.14). Neither AlAs nor AlGaAs absorbs at 800 nm. A thin AlGaAs layer of a few nanometers' thickness is buried in the topmost layer of this stack, acting as a quantum well with a strong absorption at 800 nm. At low laser intensities, a typical SBR has a reflectance of 95%, whereas under modelocked intensities the reflectance rises to

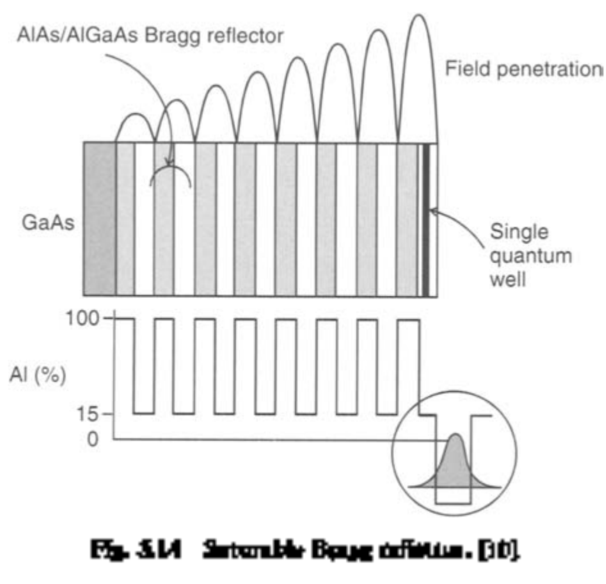

Fig. 3.14 Saturable Bragg reflector. [10]

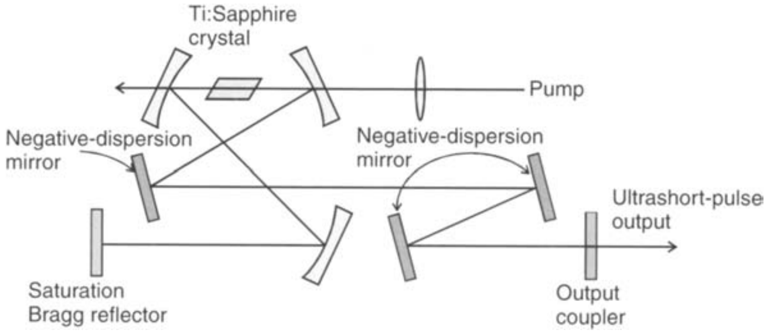

Fig. 3.15 Laser design of <30-fs Ti:sapphire that incorporates a saturable Bragg reflector [11].

almost 99%. Because of the multipass nature of a cw laser, this 4% change is more than sufficient to induce strong modelocking. Because of the absorption at 800 nm the saturable Bragg reflector has been applied in commercial Ti:sapphire laser technology in recent years. The saturable Bragg reflector method provides reliable, easy-to-use modelocked lasers for both laboratory and industrial applications. Figure 3.15 shows one of many commercial designs in which the Ti:sapphire oscillator and a solid-state pump laser are packaged in a single, compact sealed box.

We will now discuss the most common method of modelocking—*Kerr-lens modelocking* (KLM). This method requires no additional passive or active elements to modelock, and is employed in most solid-state lasers. A combination of a hard aperture and the Kerr effect leads to amplitude modulation of the resonator modes, with the frequency corresponding to the double round-trip time which is required to achieve modelocking. The Kerr effect, which has been known for a long time in nonlinear optics, implies that a refractive index is a function of a light intensity, I,

$$n = n_0 + n_2 I. \tag{3.28}$$

It indicates that the Kerr effect leads to the intensity-dependent modulation of the laser beam profile. Indeed, for a Gaussian beam profile in the transverse direction the spatial index-distribution can be written as

$$n(r) = n_0 + n_2 I(r) \tag{3.29}$$

where $I(r)$ is given by Gaussian distribution $I(r) = \exp(-pr^2)$.

Figure 3.16 shows the refractive-index distribution along the x-axis for the Gaussian beam propagating along the z-axis. One can see that the index modification in an active medium follows the intensity of the laser beam. For a positive term n_2, the index has a maximum at $x = 0$ for the centre of the Gaussian beam, and is much smaller at the wings. Therefore, the refraction index is not homogeneously distributed in the Kerr medium, and corresponds to a situation as by inserting an additional material in a shape of a Gaussian lens into an optical resonator. The refractive-index lens formed in the Kerr medium focuses the laser beam towards a centre, as illustrated in Fig. 3.17. If we introduce an aperture into a resonator, it begins to act as a selective "shutter".

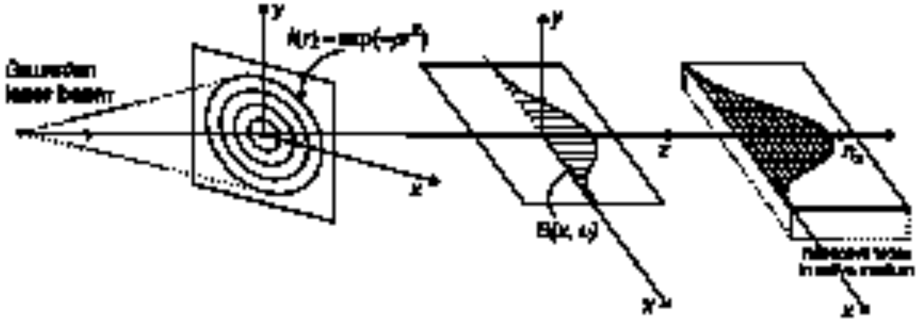

Fig. 3.16 Illustration of intensity-dependent refractive-index lens in an active medium.

This preferentially induces more loss at the edge of the beam, which is still a continuous wave, allowing the pulsed central mode to monopolize the laser gain. The modes of higher intensity are transmitted through the aperture because of the smaller size (due to the stronger Kerr lens focusing), whereas the modes of lower intensity cannot pass to the mirror M2 through the aperture, and they are lost. The high-intensity beam is reflected from the mirror M2 with some losses at the aperture, and passes through the active medium again, where is amplified. The loss–amplification process is repeated during every round-trip, leading to the amplitude modulation of the modes in the resonator, and during the modelocking.

The "shape" of the lens changes during the propagation of a pulse through a material and with the intra-cavity intensity. It can be shown, [12] that a focal length, f, is governed by the following expression

$$f = \frac{w^2}{4 n_2 I_0 L}, \tag{3.30}$$

where w is the beam waist, n_2 is the non-linear index in eq. (3.29), I_0 is the peak intensity, and L is the length of the active medium. This kind of modelocking is called, *self-modelocking*, because the Kerr-lens medium can be the laser crystal itself. Actually, the self-modelocking does not require any additional passive or active elements in the resonator. Even the hard aperture for the mode selection on the this basis is not necessary, because the natural aperture is formed by the gain profile within the lasing material. For details, the reader is referred to ref. [13]. The KLM

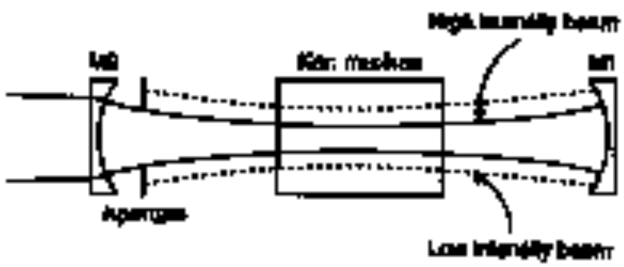

Fig. 3.17 Kerr lens amplitude modulation in an optical resonator.

effect has the result that in practically all solid-state lasers (Cr:YAG, Pr:YLF, Ti:sapphire) the modelocking is generated spontaneously without any additional modulating devices, because the active medium itself plays a role of the modulator. This kind of modelocking is commonly employed in Ti:sapphire ($Ti:Al_2O_3$) oscillators for the generation of femtosecond pulses of excellent reliability and great stability from pulse to pulse. They have been available commercially since 1990. However, in order to produce pulses which are stable and repeatable, with a strictly defined shape, one should apply devices controlling the *group velocity dispersion*—the *GVD*. The GVD effect will be discussed in Chapter 5.6.

It often happens that picosecond and femtosecond lasers using exclusively the KLM effect can become unstable owing to changes of temperature in the environment, vibrations in the laboratory, and other uncontrolled factors. Therefore, some manufacturers choose a method combining KLM and the active modelocking by an acousto-optic device. This type of modelocking is called, *regenerative modelocking*. When a solid-state laser begins to operate in the continuous work (*cw*) regime, the longitudinal modes are produced at frequencies that differ by $\Delta\nu = c/2L$. The modes are not well coupled at the beginning, and the phase difference between them changes chaotically. However, a small number of modes is partially correlated and the frequency $\Delta\nu = c/2L$ begins to modulate the beam intensity at the initial step of laser emission. This modulation frequency is recorded by a photodiode, amplified, and sent to an acousto-optic modulator. The modulator begins to modulate an active medium at the frequency that had been received from the photodiode. This solution removes the main limitation of the active modelocking which depends on the resonator cavity length, L. In the regenerative modelocking method, the signal is sent automatically to the acousto-optic transducer to change the frequency of modulation when the length of the resonator is changed a little for any reason. A detailed description of the regenerative modelocking can be found in ref. [14] and an advanced discussion of modelocking can be found in excellent tutorial presentations in refs. [13–19].

3.5. Q-SWITCHING

The peak power of a laser depends both on the pulse's duration and its energy. The shorter the duration of the pulse, and the higher its energy, the higher is the peak power. For continuous-wave modelocking, the ultimate limit of pulse duration for a Ti:sapphire laser is about 3 fs, with the typical energy of a single pulse being a few nJ, giving a peak power in the range of MW. Chirped-pulse amplification techniques, which will be discussed in Chapter 6, may help to achieve peak powers greater than TW in typical commercial configurations. However, the average power in such systems is low—typically about 1 W. In commercial systems, with a repetition of 1 kHz, the amplified pulse energy is 1 mJ and the average power is 1 W.

Not all applications require cutting-edge performance, and the ultrafast Ti:sapphire systems are still complex and expensive devices. Another technique, called *Q-switching*, is employed to generate short pulses; this does not permit the generation of femtosecond pulses, but is very useful for the generation of picosecond or nanosecond pulses of high energy. The most powerful laser that employs the

Q-switching technique (Nd:glass) has achieved the peak power greater than a petawatt.

The Q-switching method takes its name from the resonator quality factor Q discussed in Chapter 2.2. The quality factor, Q is defined as the ratio of the energy stored in the cavity to the energy loss per cycle. We will show that by a fast change of Q we can force a laser to produce pulses. The pulses produced with the Q-switching technique are longer (picosecond, nanoseconds) than those obtained with modelocking (femtoseconds), but they have much higher energy. For typical femtosecond modelocked lasers the energy of a single pulse is around a few nJ at the high repetition rate of 76–82 MHz, whereas for the Q-switched pulses the typical energy of a single pulse is a few mJ at a repetition of a few Hz.

In Q-switching, the energy is stored in the optical cavity, with the population inversion building up until the Q-switch is activated. Once the Q-switch is activated, the stored energy is released in a single pulse. The higher the quality factor, the lower are the losses, and the more energy can be stored inside the cavity. In the Q-switched lasers, the energy obtained from the population inversion by pumping (usually flash lamps) is stored in the active medium. Although the stored energy is far above the threshold for lasing action, the action does not start, being prevented by introducing controlled losses to the resonator (low Q). So, the gain in the resonator is high, but the cavity losses are also high and the laser does not lase. The energy may be stored in the upper level as long as the pumping pulse from the flash lamp builds up and the relaxation processes do not drop the molecules back to the ground state and destroy the population inversion. This time is of the order of the lifetime of the upper state. Once the Q-switch is activated, and the high quality factor Q is restored, the lasing suddenly starts and the stored energy is released in a single short pulse. The peak power of such a pulse is extraordinarily high.

The mechanism of generation of a Q-switched pulse is illustrated in Fig. 3.18, and the theory of the Q-switch is given in refs. [20–22]. Here we only present the equation derived in ref. [20] for the pulse duration in a three-level system for rapidly Q-switched lasers,

$$\Delta t_p = \tau_c \frac{n_i - n_f}{n_i - n_t\left[1 + \ln\left(\frac{n_i}{n_t}\right)\right]} \tag{3.31}$$

where τ_c is the photon lifetime. n_i, n_t, n_f are respectively the initial, the threshold value, and the final population inversion densities.

Now, when we understand the major steps in the mechanism of generation of Q-switched pulses we need to ask how to control the resonator quality-factor, Q, and how to switch rapidly between the low and high values of Q. There are several methods, including acousto-optic, electro-optic, mechanical, and dye switches. The idea of the acousto-optic modulator was explained in Chapter 3.2. We presented the acousto-optic modulator employed in the active modelocking and showed that the active modelocker usually works in the Raman–Nath regime (eq. 3.26), in contrast to the Bragg regime (eq. 3.27) that is employed in the cavity dumper and in the Q-switching modulators. The main difference between these regimes is presented in Fig. 3.19.

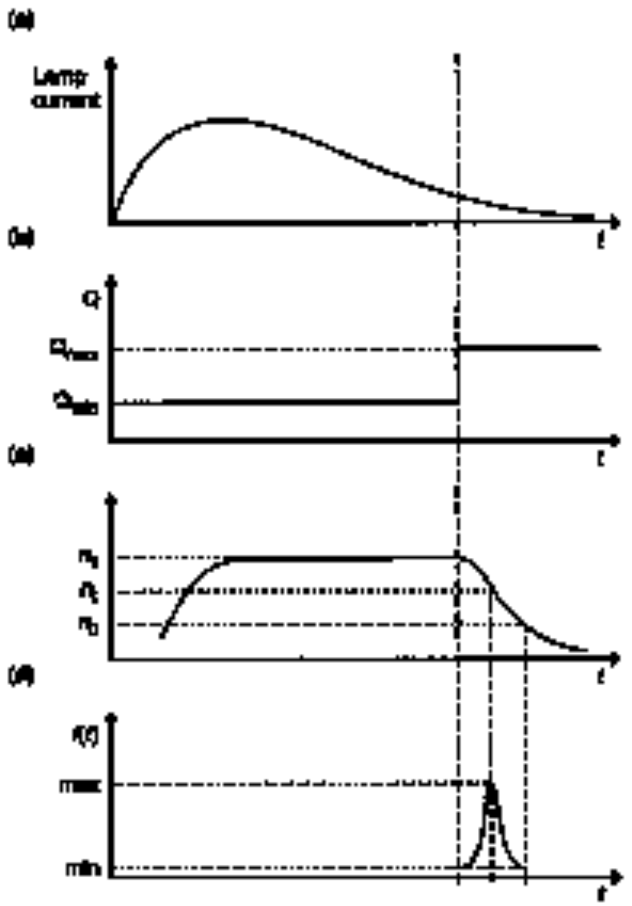

Fig. 3.18 Mechanism of generation of a Q-switched pulse: (a) pumping, (b) Q-switching, (c) energy storage in a three-level system, (d) pulse generation.

Briefly, an acousto-optic switch consists of a block of optical material (quartz, fused silica SiO_2, flint glass, tellurium dioxide) that is transparent to the laser beam. A piezoelectric transducer, usually a crystal such as lithium niobate, is bonded to one side of the block by epoxy or vacuum metallic bonding. The radiofrequency (RF) driver generates in the transducer the acoustical wave that propagates through the medium. The radiation inside the resonator interacts with the sound wave leading to diffraction of the incident beam. Compared to the Raman–Nath regime presented in Chapter 3.2, the frequency of the acoustic wave is higher, the interaction path is lengthened, and higher-order diffraction is eliminated. Only zero and first order rays are not suppressed. The diffracted beam reduces the quality of the resonator, Q, allowing the energy to build up and store inside the resonator without lasing. When the sound-wave stops travelling (the transducer is switched off) the radiation beam is no longer diffracted (high Q), the laser begins to lase, and the energy is released from the resonator in a single pulse.

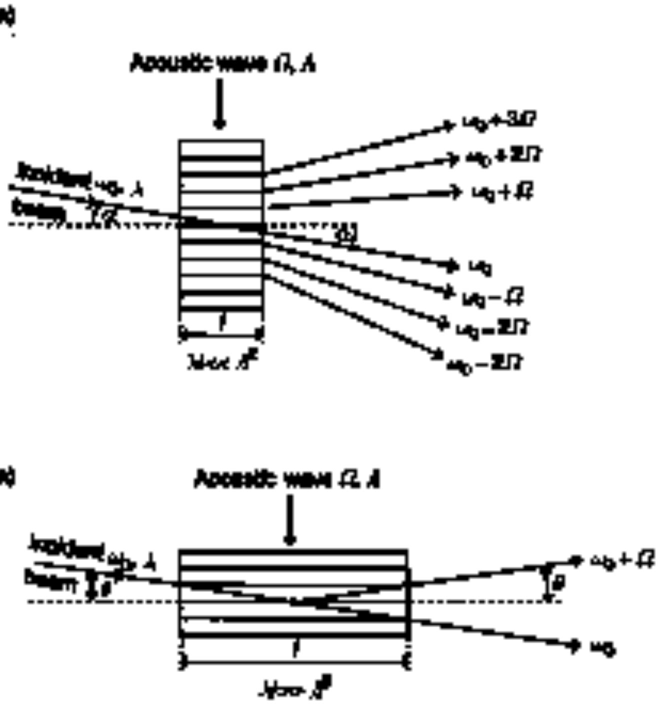

Fig. 3.19 Limit cases of acousto-optic devices: (a) Raman–Nath regime; (b) Bragg regime.

Several criteria must be taken into account in choosing a proper Q-switch:

1. the upper-state lifetime; only lifetimes long enough to prevent spontaneous energy emission can be Q-switched;
2. the gain parameter; if the gain is high, the diffracted light may not be able to prevent a feedback in the cavity leading to laser lasing;
3. the storage capacity, which denotes how much power the Q-switch will have to accommodate.

The Q-switching is employed in flash lamp-pumped solid-state lasers and diode-pumped solid-state lasers such as Nd:YAG, Nd:YVO$_4$, Nd:YLF, as well as ruby and Nd:glass.

3.4. CAVITY DUMPING

Cavity dumping is not a technique for generation of ultrashort pulses. It is usually used to increase the pulse energy or change the repetition rate. We will discuss cavity dumping in this Chapter because we want to compare it with the Q-switching technique, and to illustrate similarities and important distinctions.

The author's experience is that beginners find it difficult to understand the difference between *Q*-switching and cavity dumping. In both cases, energy is stored in the resonator cavity—often with the help of the acousto-optic devices working in the same Bragg regime. What distinguishes and provides the specificity of these methods? In the *Q*-switching regime, the energy is "stored" in the population inversion—in the amplifying medium. During energy storing, shortly before the energy is released from the cavity, the laser does not lase, because the cavity is kept below the threshold conditions. Although the gain in the active medium is high, the cavity losses (low *Q*) are also high, preventing lasing action.

In contrast, in the cavity dumping mode the cavity is not kept below the threshold conditions, and the laser lases all the time (both when it emits pulses or does not), because the energy is stored in the optical radiation energy inside the cavity, and not only in the population inversion. The only threshold that must be kept is the damage threshold for the optical elements inside the cavity. Cavity dumping can be employed in any dye laser or solid-state laser. The cavity dumping can be employed in cw-pumped lasers, flash-lamp pumped lasers, and lasers pumped with modelocked lasers.

Cavity dumping, like *Q*-switching, can significantly increase the pulse energy of a modelocked laser. In contrast to *Q*-switching, which produces a burst of modelocked pulses within the envelope of a 100–200 ns *Q*-switch pulse, the cavity-dumped laser produces a single modelocked pulse (Fig. 3.20).

The other function of cavity dumpers is to change the repetition rate. Cavity dumping of continuously pumped lasers is a way to obtain pulses of higher repetitions (from kHz to MHz) than those available by *Q*-switching. For example, repetition rates from 125 kHz to several MHz were achieved with cavity dumping for Nd:YAG lasers pumped by cw-sources [23, 24]. In contrast, cavity-dumped dye lasers, pumped with *Q*-switched and modelocked pulses from Nd:YAG lasers at 76 MHz repetition, can change the high repetition to lower repetition of a few hundreds of kHz. To help the understanding of cavity dumping we will

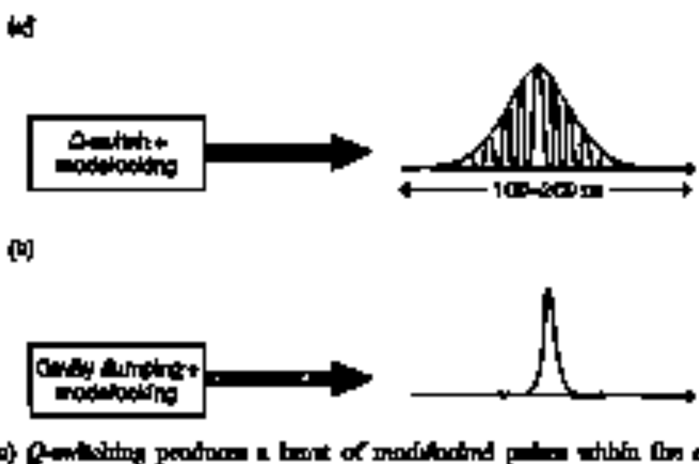

Fig. 3.20 (a) *Q*-switching produces a burst of modelocked pulses within the envelope of a 100–200 ns *Q*-switch pulse; (b) cavity dumped laser produces a single modelocked pulse.

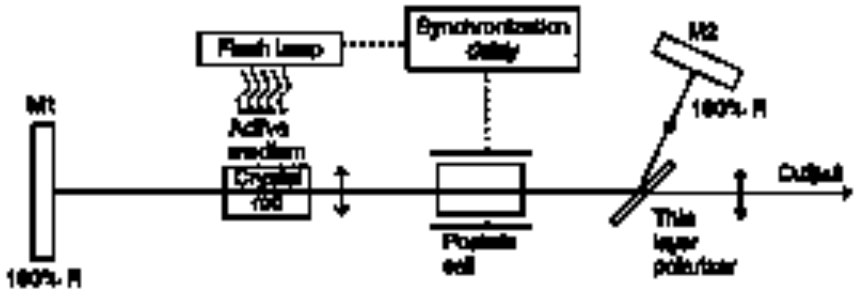

Fig. 3.21 Optical layout for cavity dumping. The arrow ↕ illustrates the polarization in the plane of the drawing; ● – polarization perpendicular to that plane.

explain it for a simple configuration based on an electro-optic device (Pockels cell). Later we will discuss the cavity dumping with an acousto-optic device for mode-locked lasers.

The typical optical layout for cavity dumping is presented in Fig. 3.21.

The flash lamp is fired at $t=0$, and its intensity begins to increase, producing fluorescence in the active medium. The horizontally polarized fluorescence (in the plane of the drawing in Fig. 3.21) passes through the thin layer polarizer as lost output light. Upon reaching the maximum lamp-current ($t_1 \sim 0.8$ ms) and peak energy storage (and maximum population inversion) in the crystal, the Pockels cell ($\lambda/2$) is switched on at t_1, changing the polarization of the light to the vertical plane. The resulting vertically polarized light is reflected, and not transmitted, by the thin-layer polarizer, and reflected by the 100% R mirror, M2. Therefore, the beam is kept inside the cavity, leading to energy storage. When the power in the cavity reaches its peak value at t_2 ($\Delta t \sim t_2 - t_1 \approx 60$ ns for the ruby laser [23]) the Pockels cell is switched off and the polarization returns to the horizontal. The energy stored in the cavity can now be released through the thin-layer polarizer as an output pulse. This takes roughly the round-trip time, which is required to completely drain the energy from the cavity. Thus, the pulse-duration of the cavity-dumped pulse is almost completely determined by the round-trip time, which depends on the resonator geometry. If we assume a 1 m long cavity, the pulse duration, $t_p = 2L/c \approx 6.7$ ns. Therefore, the combination of the Pockels cell, thin-layer polarizer, and 100% mirror M2, leads to energy storage inside the cavity during the time Δt between switching the Pockels cell on and off, when the energy builds up. Within this time of ~60 ns the light passes through the resonator about 60 ns/$t_p \approx 12$ times. Without cavity dumping, it would be released every round-trip time.

We shall now discuss cavity dumping for modelocked lasers employing an acousto-optic device to store the energy inside a cavity. We follow the excellent explanation presented in ref. [1].

In Fig. 3.22 is shown a typical cavity dumper employing an acousto-optic device (Bragg cell). The operation of the acousto-optic modulator operating in the Bragg regime is explained above (Fig. 3.19b). This configuration is often used in dye lasers pumped by the Q-switched, modelocked Nd:YAG lasers.

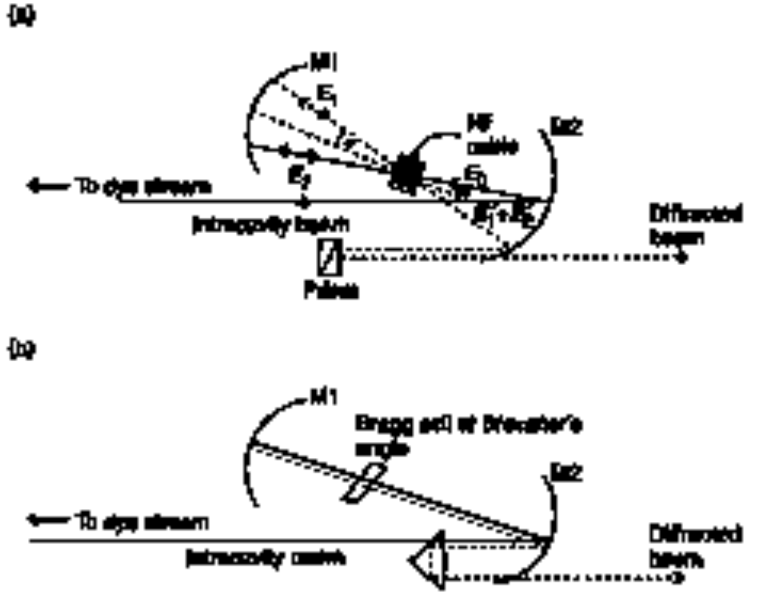

Fig. 3.22 The configuration of a cavity dumper: (a) top view, (b) side view.

In the vertical plane (side view) the Bragg cell is oriented at Brewster's angle, to minimize reflective losses and favour lasing of vertically polarized light. In the horizontal plane (top view) the Bragg cell is oriented at the Bragg angle θ ($\sim 2.3°$ from the normal for $\lambda = 600$ nm, and acoustic frequency $\Omega = 779$ MHz). The incident radiation (E_0) is split into one diffracted beam (E_1) and one directly transmitted beam, after crossing the modulator (E_2). The two beams are sent back upon themselves, since the acousto-optic cell is placed at the center of curvature of the spherical mirror M1. They cross for a second time in the modulator. Part of the reflected light is sent back in the incident direction (E_0) to the resonator cavity, and the part corresponding to the directly transmitted beam ($E_1 \to E_1'$) plus the diffracted part of E_2 (E_2'), is sent out of the cavity ($E_1' + E_2'$). We now calculate the output field ($E_1' + E_2'$).

The incident field E_0 is described by:

$$E_0 = A_0 \exp[i\omega t], \tag{3.32}$$

where ω is the frequency of the incident laser beam. The acoustic field in the Bragg cell is written as:

$$E_s = A_s \exp i(\Omega t + \phi_s), \tag{3.33}$$

where Ω and ϕ_s are respectively the frequency and the phase of the sound wave. The two fields (E_1 and E_2) after the first passage of the Bragg cell are given by

$$E_1 = E_0 \sqrt{\eta} \exp[i(\omega - \Omega)t] \exp[i(\pi/2 - \phi_s)] \exp(i\phi_1) \tag{3.34}$$

$$E_2 = E_0 \sqrt{1 - \eta} \exp[i(\omega t - \phi_2)]. \tag{3.35}$$

The terms ϕ_1 and ϕ_2 are the phase changes for the two beams travelling through the Bragg cell at the exit plane of the cell, and are functions of the geometry of the Bragg cell. The additional phase $\pi/2$ originates from the fact that the electric field is a transverse wave, in contrast to the longitudinal acoustic wave. Thus, the interaction between them is shifted in phase by $\pi/2$. The term η characterises losses by diffraction in one passage across the Bragg cell

$$\eta = \frac{I_{diff}}{I_{in}}, \tag{3.36}$$

where I_{diff} and I_{in} are respectively the intensity of the diffracted- and the incident light. Since the intensity I is proportional to the square of the electric field E, the terms $\sqrt{\eta}$ and $\sqrt{1-\eta}$ appear in eqs. (3.34) and (3.35). The parameter η characterising the diffraction efficiency depends on the acoustic power, the geometry of the acousto-optic device, and characteristics of the material. The fields after the second crossing of the Bragg cell are written as

$$E_1' = E_0\sqrt{\eta}\sqrt{1-\eta}\exp[i(\omega-\Omega)t]\exp[i(\pi/2-\phi_a)]\exp[i(\phi_1+\phi_1')] \tag{3.37}$$

$$E_2' = E_0\sqrt{\eta}\sqrt{1-\eta}\exp[i(\omega-\Omega)t]\exp[i(\pi/2-\phi_a)]\exp[i(\phi_2+\phi_2')], \tag{3.38}$$

where ϕ_1' and ϕ_2' are the phase changes during the round trip. The resulting field $(E_1'+E_2')$ that is sent out of the cavity can be written as

$$\begin{aligned} E_{out} &= E_1' + E_2' \\ &= 2E_0\sqrt{\eta}\sqrt{1-\eta}\exp[i(\omega t+\pi/2)]\{\exp[-i(\Omega t+\phi_a-\phi_1)]\exp[i(\Omega t+\phi_a-\phi_2)]\} \end{aligned} \tag{3.39}$$

where $\phi_1 = \phi_1 + \phi_1'$; $\phi_2 = \phi_2 + \phi_2'$. By combining these equations we obtain

$$E_{out} = 2E_0\sqrt{\eta}\sqrt{1-\eta}\exp[i(\omega t+\pi/2)]\exp\left(i\frac{\phi_1+\phi_2}{2}\right)[\cos(\Omega t+\phi_a+\phi_2-\phi_1)] \tag{3.40}$$

and the corresponding intensity,

$$I_{out} = |E_{out}|^2 = 4E_0^2\eta(1-\eta)[1+\cos 2(\Omega t+\phi_a+\phi)]; \tag{3.41}$$

where $\phi = \frac{\phi_2-\phi_1}{2}$.

The expression (3.41) shows that the diffracted intensity, I_{out}, is modulated according to twice the acoustic wave frequency Ω. It has maximum values for times t given by

$$\Omega t + \phi_a + \phi = k \tag{3.42}$$

where k is an integer, and a minimum for t given by

$$\Omega t + \phi_a + \phi = k + \frac{1}{2}. \tag{3.43}$$

The result obtained for the output intensity, I_{out}, simply says that the two diffracted beams $E_1' + E_2'$ can interfere with each other either, constructively or destructively, depending on the phase-relationship between the acoustic wave ϕ_s and the light beam in the laser ϕ. Additionally, the term $4\eta(1-\eta)$ in eq. (3.41) explains why the double passing across the Bragg cell is preferred. If we assume $\eta = 0.5$ for a single-pass intensity diffraction, the double pass gives 100% efficiency. Therefore, it is possible to time the acoustic pulse in the Bragg cell relative to the phase of the laser pulse such that either a maximum intensity is deflected out of the beam, or essentially no intensity at all—destructive interference prevents the light from being deflected. This method is often called "*integer plus* $\frac{1}{2}$ *timing*", and can be used to lower the repetition of the dye laser pumped by the high-repetition modelocked lasers. This can be done simply by properly choosing of the acoustic frequency with respect to the modelocked laser repetition. If the acoustic frequency is chosen in such a way that dividing it by the modelocking frequency yields an integer k plus $\frac{1}{2}$, every

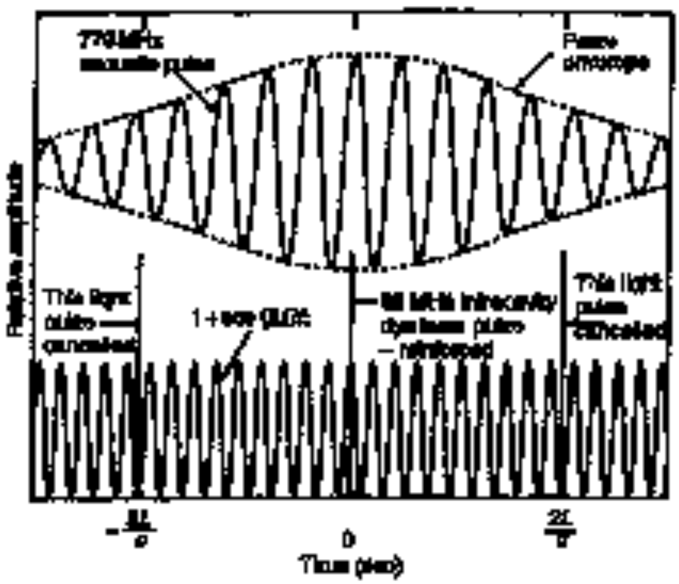

Fig. 3.23 A diagram illustrating *integer plus* $\frac{1}{2}$ *timing* in the cavity dumper. Three adjacent mode-locked dye laser pulses are illustrated in the bottom part of the Figure. Since the repetition rate of the laser is 82 MHz, they are separated in time by $2L/c$, or about 12.2 ns, where L is the optical cavity length of the dye laser. The acoustic pulse, which is sent through the Bragg cell by the transducer, is illustrated in the top part of the Figure. Its frequency is chosen to be 779 MHz which, when divided by the repetition rate, yields $9\frac{1}{2}$—an integer plus $\frac{1}{2}$. Owing to the double pass configuration in the cavity dumper, the dye laser output consists of two light beams, one shifted to higher frequency by the acoustic frequency, and one shifted down. They then interfere with one another in a manner which modulates the output at a frequency twice that of the acoustic wave. This modulation function is shown in the bottom part of the Figure. It shows how the output of the laser would be modulated if the laser were operated with continuous light, rather than being modelocked. Depending on the time of arrival of the intra-cavity dye laser pulse relative to that of the acoustic pulse, the output pulse is either reinforced or cancelled. Reproduced from ref. [1]

k-modelocked pulse will be sent out with a maximum intensity; the other pulses will not be sent out, because their intensity will be zero. Figure 3.23 illustrates integer plus $\frac{1}{2}$ timing in the cavity dumper [1].

REFERENCES

1. E.W. Small, *Topics in Fluorescence Spectroscopy*, vol. 1, J.R. Lakowicz, ed., Plenum Press, New York (1991)
2. M. Born, E. Wolf, *Principles of Optics*, Pergamon Press, Oxford (1965)
3. P. Debye, F.W. Sears, *On the Scattering of Light by Supersonic Waves*, Proc. Natl. Acad. Sci. USA 18 (1932) 409–414
4. H.W. Mocker, R.J. Collins, *Mode Competition and Self-locking Effects in a Q-switched Ruby Laser*, Appl. Phys. Lett. 7 (1965) 270–272
5. A.J. DeMaria, D.A. Stetser, H. Heynau, Appl. Phys. Lett. 8 (1966) 174–176
6. D. von der Linde, Appl. Phys. Lett. 2 (1973) 281
7. G. Gianni, M. Mischen, IEEE J. QE-9 (1973) 979
8. D. von der Linde, K.F. Rodgers, IEEE J. QE-9 (1973) 960
9. U. Keller, D.A.B. Miller, G.D. Boyd, T.H. Chiu, J.F. Ferguson, M.T. Asom, Opt. Lett. 17 (1992) 505
10. S. Tsuda et al., IEEE J. Sel. Topics in Quant. Elect. 2 (1996) 454
11. B. Craig, A. Krueger, *Saturable Bragg Reflectors Simplify Modelocking*, Laser Focus World 36 (8) (August, 2000) 227–228
12. M. Piché, Opt. Commun. 86 (1991) 156
13. F. Krausz, M.E. Fermann, T. Brabec, P.F. Curley, M. Hofer, M.H. Ober, C. Spielmann, E. Wintner, A.J. Schmidt, IEEE J. QE-28 (1992) 2097
14. J.D. Kafka, M.L. Watts, J.W.J. Pieterse, *Picosecond and Femtosecond Pulse Generation in a Regeneratively Mode-Locked Ti:Sapphire Laser*, IEEE J. Quant. Electron. 28 (1992) 2151
15. W. Koechner, *Solid-State Laser Engineering*, 5th Edition, vol. 1, Springer-Verlag (1999)
16. H.A. Haus, J.G. Fujimoto, E.P. Ippen, IEEE J. QE-28 (1992) 2086
17. E.P. Ippen, H.A. Haus, L.Y. Liu, J. Opt. Soc. Am. B 6 (1989) 1736
18. S.L. Shapiro (ed.), *Ultrashort Laser Pulses*, Topics Appl. Phys., vol. 18, Springer, Berlin, Heidelberg (1977)
19. W. Kaiser (ed.), *Ultrashort Laser Pulses*, 2nd edn., Topics Appl. Phys., vol. 60, Springer, Berlin, Heidelberg (1993)
20. W.G. Wagner, B.A. Lengyel, J. Appl. Phys. 34 (1963) 2040
21. R.B. Kay, G.S. Waldman, J. Appl. Phys. 36 (1965) 1319
22. J.J. Degnan, IEEE J. QE-25 (1989) 214
23. D. Maydan, R.B. Chesler, *Q-Switching and Cavity Dumping of Nd:YAlG Lasers*, J. Appl. Phys. 42(3) (1971) 1031–1034
24. R.B. Chesler, D. Maydan, *Calculation of Nd:YAlG Cavity Dumping*, J. Appl. Phys. 42(3) (1971) 1028–1030
25. L.P. [illegible], V.A. [illegible], V.V. [illegible], Sov. Phys. 14 (1965) 603